

GALEX J184559.8–413827: a new extreme helium star identified using SALT*

C. Simon Jeffery^{1,2†}

¹Armagh Observatory and Planetarium, College Hill, Armagh BT61 9DG, UK

²School of Physics, Trinity College Dublin, College Green, Dublin 2, Ireland

Accepted Received . . . ; in original form . . .

ABSTRACT

A high-resolution spectrum of the helium-rich ‘hot subdwarf’ GALEX J184559.8–413827 (J1845–4138) obtained with SALT HRS demonstrates it to be the first extreme helium (EHe) star to be discovered in nearly 40 years. A quantitative analysis demonstrates it to have an atmosphere described by $T_{\text{eff}} = 26\,170 \pm 750$ K, $\log g/\text{cm s}^{-2} = 4.22 \pm 0.10$, and a surface chemistry characterised by CNO-processed helium, a 1% contamination of hydrogen (by number), and a metallicity 0.4 dex subsolar. Its distance and position are consistent with membership of the Galactic bulge. Its sharp absorption lines place strong constraints on both the rotation and microturbulent velocities. Spectroscopically, J1845–4138 closely resembles the pulsating EHe star V652 Her, generally considered to be the product of a double helium white dwarf merger evolving to become a helium-rich sdO star.

Key words: stars: abundances, stars: fundamental parameters, stars: chemically peculiar, stars: individual (GALEX J184559.8–413827, V652 Her)

1 INTRODUCTION

Extreme helium stars (EHes) comprise some seventeen stars of spectral types equivalent to A and B but having weak or no hydrogen Balmer lines. In their place, relatively sharp and strong lines of neutral helium indicate low surface gravities and atmospheres dominated by helium. The next most abundant elements are carbon, nitrogen and oxygen, indicative of highly processed material exposed at the stellar surface. The first extreme helium star, HD124448, was identified by Popper (1942). This was followed by discoveries spanning some thirty years, many arising from spectroscopic surveys of luminous blue stars. All of these have been analysed spectroscopically in more or less detail, giving effective temperature and surface gravities; a full list is provided by Jeffery (2008), to which should be added analyses of BD+10°2179 by Pandey & Lambert (2011) and Kupfer et al. (2017). Translating surface gravity into luminosity-to-mass ratio (L/M), the class covers a range of nearly 2 dex in L/M , with the brightest members lying close to the Eddington limit. Hence, the fact that there have been no new luminous EHes discovered since about 1980 (Drilling & Hill 1986) is easily understood. With sur-

veys of luminous blue stars complete to $B = 12$ for the Milky Way and for $b = \pm 30^\circ$ and $l = \pm 60^\circ$ (Drilling & Bergeron 1995; Drilling 1996), fainter EHes would either lie well outside the Milky Way or be heavily obscured and reddened by its central bulge. At the least luminous end of their range, EHe stars have surface gravities similar to those seen on the main-sequence. The EHes appear to be substantially less numerous.

Since all of the classical EHes were discovered, there have been numerous spectroscopic surveys for *faint* blue stars (sometimes masquerading as quasar or galaxy surveys), including the Palomar-Green (Green et al. 1986), Hamburg quasar and Hamburg/ESO (Hagen et al. 1995; Wisotzki et al. 1996), Edinburgh-Cape (Stobie et al. 1997), HK (Beers et al. 1992), Sloan (York et al. 2000) and GALEX (Bianchi et al. 2014) surveys. Each adopted a scheme to classify the spectra of stellar objects and thereby identified many new and interesting stars. Drilling (1996) recognized that the class identified by Green et al. (1986) as sdOD (“pure He I absorption spectra, characterized by the weakness or absence of hydrogen Balmer lines and He II 4686 while showing the singlet He I 4388 about equal in strength to the triplet He I 4471”), and by Moehler et al. (1990) as He-sdB, is the same definition as that given for extreme helium stars and binaries by Drilling & Hill (1986). Yet no new EHe stars were found.

The sdOD/He-sdB classification also embraces helium-

* based on an observation made with the Southern African Large Telescope (SALT)

† email: csj@arm.ac.uk

rich stars of higher surface gravity, i.e. helium-rich hot subdwarfs. Considerable effort has been spent on discovering and exploring these stars, with spectacular results. They turn out to fall into diverse groups, including the double subdwarf PG1544+488 (Schulz et al. 1991; Ahmad et al. 2004; Şener & Jeffery 2014), the binary CPD-20°1123 (Naslim et al. 2012), through the chemically-peculiar intermediate helium subdwarfs (Naslim et al. 2011, 2013; Jeffery et al. 2017), the low-gravity He-sdO stars and O(He) stars (Husfeld et al. 1989; Reindl et al. 2014) to the high-gravity extreme helium sdO stars (Greenstein & Sargent 1974; Dreizler et al. 1990; Ströer et al. 2007; Naslim et al. 2010; Justham et al. 2011; Zhang & Jeffery 2012). Drilling (1996) and Drilling et al. (2013) introduced an MK-like classification scheme which clearly distinguishes between helium-rich subdwarfs and extreme helium stars, but requires a resolution closer to 1.5\AA than the 10\AA of many surveys. Hence, survey spectra have rarely been classified using the Drilling scheme¹. Stars of interest to us have more frequently been classified as He-sdB, He-sdOB, or He-sdO

Efforts to find more examples of some subclasses require high-resolution and high signal-to-noise spectra to identify weak and double lines. A spectroscopic survey of stars classified as helium-rich subdwarfs, especially He-sdB or sdOD using 8m class telescopes has been undertaken. This paper reports an observation of one such star obtained with the high-resolution spectrograph (HRS) on the Southern Africa Large Telescope (SALT) (Buckley et al. 2006; Bramall et al. 2010; Crause et al. 2014)

2 OBSERVATIONS

GALEX J184559.8–413827 ($\alpha_{2000} = 18^{\circ}45'59.8''$, $\delta_{2000} = 41^{\circ}38'27''$, $V = 14.6$: J1845–4138 hereafter) was identified to be a faint blue star from GALEX colours by Vennes et al. (2011). A flux-calibrated low-resolution spectrum obtained with the Faint Object Spectrograph and Camera mounted on the European Southern Observatory’s New Technology Telescope (EFOSC2/NTT) on 2008 October 21 was classified ‘He-sdB’, being dominated by neutral helium lines. A coarse analysis of the spectrum and colours yielded first an effective temperature $T_{\text{eff}} = 36\,400 \pm 3\,200$ K, surface gravity $\log g/\text{cm s}^{-1} = 5.75 \pm 0.65$, and surface helium-to-hydrogen ratio > 0.40 (Vennes et al. 2011), and second $T_{\text{eff}} = 35\,930^{+840}_{-4770}$ K, $\log g/\text{cm s}^{-1} = 5.75^{+0.27}_{-0.23}$, $\log n_{\text{He}}/n_{\text{H}} = 2.10^{+1.10}_{-0.38}$ (Németh et al. 2012). Both studies used the same observations; the first used atmospheres comprising hydrogen and helium only, but in which departures from local thermodynamic equilibrium were considered (non-LTE), while the second used non-LTE models comprising hydrogen, helium, carbon, nitrogen and oxygen. The latter also provided weak upper limits for the CNO abundances relative to hydrogen of 15%, 75% and 22% respectively.

The ‘He-sdB’ classification led to the inclusion of J1845–4138 on a target list for observations of chemically-peculiar hot subdwarfs with the SALT HRS. One observation was obtained at UTC 02:24 on 2017 March 17 with

a median seeing of $1.3''$. Two exposures were obtained in each of the HRS cameras, the first with an exposure time of 1300 s, the second was terminated after 700 s by a technical problem. A second observation was attempted the following night, but the wrong star was observed.

The HRS spectrum was reduced to 1-dimension (total counts versus wavelength) object and sky orders using the SALT HRS pipeline² (Crawford et al. 2016). Flux calibration was not attempted. The wavelength ranges covered by the spectra are $3860 - 5519 \text{\AA}$ and $5686 - 8711 \text{\AA}$ respectively, the combined spectrum having a S/N ratio in the range 20 – 30 at a resolution of $\approx 37,000$. The orders were rectified, mapped onto a common wavelength grid (equally spaced in log wavelength) and merged using an order-management tool written for échelle spectra by the author. Rectification at low exposure levels remains problematic, in the current case leading to problems at the blue end of the blue spectrum.

Fig. 1 shows that the He I absorption lines are readily apparent and everywhere stronger than the Balmer lines. He II 4686\AA , can be identified, but not the He II Pickering series. The He I lines are everywhere narrower than seen in helium-rich hot subdwarfs with $\log g \geq 5$, but less sharp than the lowest-gravity extreme helium stars. On the other hand the spectrum is remarkably *similar* to that of the better known EHe star V652 Her (Jeffery et al. 2015), including in particular the extremely rich spectrum of singly-ionized nitrogen (Fig. 1). The most marked difference is that He II 4686\AA is significantly stronger in J1845–4138, indicating a higher T_{eff} . A detailed analysis to determine the surface properties more precisely is presented in the next section.

A single value for the heliocentric radial velocity of J1845–4138 was measured by comparing the observed spectrum obtained at 2017 03 17 02h 24m (Julian Date 2457828.6000) with the best-fit theoretical spectrum, yielding a value $-66.1 \pm 0.2 \text{ km s}^{-1}$. There was no discernible shift between the two exposures. The mean value is approximately consistent with a series of five measurements made over the space of three nights in 2012 and which gave $\bar{v} = -57.6 \pm 6.1 \text{ km s}^{-1}$ (Kawka et al. 2015).

3 ANALYSIS

A grid of model atmospheres and theoretical spectra was prepared based on the approximate composition for V652 Her (Jeffery et al. 2001). The input composition for the model grid was checked for consistency with the measured abundances, and an iteration was carried out where necessary. The observed spectrum used to fit T_{eff} and g was the order-merged spectrum direct from the rectification procedure. This procedure was carefully designed to preserve the profiles of broad lines, even where they extend over substantial fractions of an order or across order overlaps. Initial estimates for T_{eff} and g were obtained using the Armagh LTE³ model atmosphere codes STERNE3, SPECTRUM and SFIT (Behara & Jeffery 2006; Jeffery et al. 2017),

² PyHRS: <http://pysalt.salt.ac.za/>

³ Local thermodynamic equilibrium was assumed throughout the analysis. Recent analyses of V652 Her and the EHe BD+10°2179 (Przybilla et al. 2005; Kupfer et al. 2017) showed departures from

¹ A recent exception used tools in the Virtual Observatory (Pérez-Fernández et al. 2016).

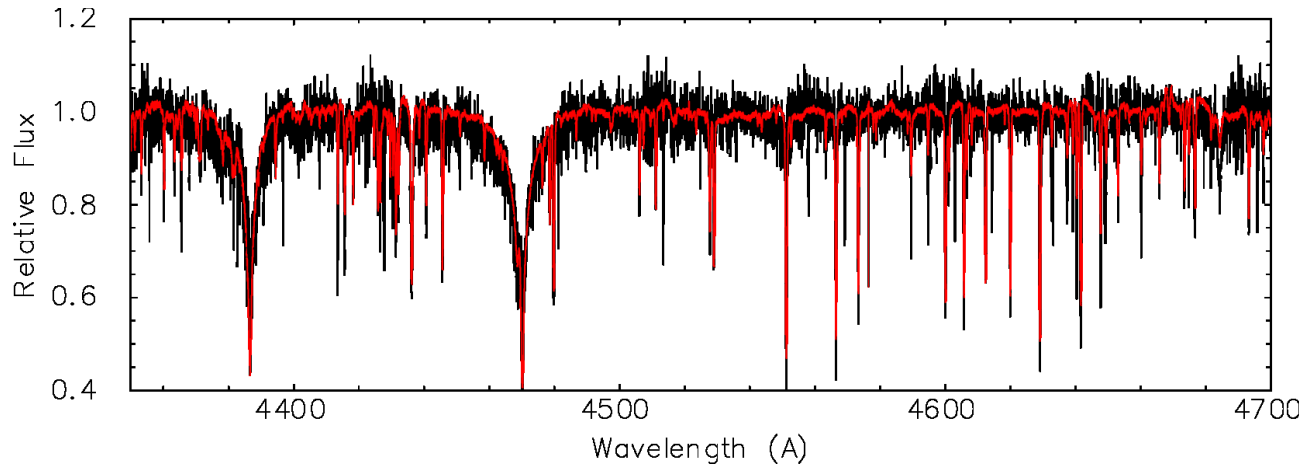


Figure 1. Part of the renormalised SALT HRS spectrum of J1845–4138 (black) compared with the median spectrum of V652 Her near maximum radius obtained by Jeffery et al. (2015, red).

Table 1. Atmospheric abundances of J1845–4138, helium stars with similar L/M ratios, and the Sun. Abundances are given as $\log \epsilon$, normalised to $\log \Sigma \mu \epsilon = 12.15$.

Star	$\log \epsilon$													Ref
	H	He	C	N	O	Ne	Mg	Al	Si	P	S	A	Fe	
J1845–4138	9.56	11.54	6.91	8.69	7.78	8.29	7.91	6.44	7.61	5.62	6.93	–	7.07	
V652 Her	9.61	11.54	7.29	8.69	7.58	7.95	7.80	6.12	7.47	6.42:	7.05	6.64	7.04	1,2
BX Cir	8.1	11.5	9.02	8.4	8.0			7.2	6.0	6.8	5.0	6.6	6.6	3
LSIV+6°2	7.3	11.52	9.41	8.54	8.30	9.35	7.34	6.26	7.11	5.99	6.99		7.10	4
HD144941	10.3	11.5	6.80	6.5	7.0			6.1	4.8	6.0			5.7	5
Sun	12.0	10.93	8.43	7.83	8.69	7.93	7.60	6.45	7.51	5.45	7.12	6.40	7.50	6

: value uncertain.

References. 1: Jeffery et al. (1999), 2: Jeffery et al. (2001), 3: Drilling et al. (1998), 4: Jeffery (1998), 5: Harrison & Jeffery (1997); Jeffery & Harrison (1997), 6: Asplund et al. (2009).

by finding the best-fit spectrum in a grid which covers the solution space $(T_{\text{eff}}/\text{kK}, \log g/\text{cm s}^{-2}, n_{\text{He}}/n_{\text{H}}) = (20(2)30, 2.8(0.2)4.4, 99)$.

The observed spectrum was further renormalised using the best-fit model so as to facilitate the measurement of abundances from narrow and weak lines (Figs. 1, A.1 – A.3). The renormalised spectrum was not used for measuring T_{eff} and g since the wings of the crucial He I lines are significantly affected by this renormalisation process.

Inspection showed that many lines were significantly sharper in the observed spectrum than in the model, with some close lines resolved in the former and not the latter. The rotation velocity was already set to zero. The instrumental profile was reduced to 0.001 \AA (full-width half-maximum), corresponding to the nominal value for medium resolution observations with HRS (37 000). In order to model the observed line splitting, the microturbulent velocity (ξ) in the model had to be reduced from 7 to 2 km s^{-1} . The value adopted for V652 Her was 9 km s^{-1} , but dynamical effects in the pulsating atmosphere probably contribute to this value. Since the microturbulent velocity contributes significantly to the metal line opacity due and hence to the temperature

structure of the model atmospheres, a new model grid was computed.

The final surface properties measured for J1845–4138 are $T_{\text{eff}} = 26\,170 \pm 750 \text{ K}$ and $\log g/\text{cm s}^{-2} = 4.22 \pm 0.10$, with $\xi = 2 \text{ km s}^{-1}$. This is compared with other EHe stars in Fig. 3. An indication of the systematic error is obtained by the reduction in ξ , which produced shifts of 30 K and 0.03 dex respectively.

Atmospheric abundances were obtained from the renormalised spectrum by χ^2 minimisation, as in the analysis of UVO 0825+15 (Jeffery et al. 2017). Given the scatter seen in line-by-line analyses, and the greater noise in the current spectrum, the abundance errors are conservatively estimated at ± 0.2 dex for each species. The best-fit abundances of observed species are given in Table 1 as $\log \epsilon$, normalised to $\log \Sigma \mu \epsilon = 12.15$, where ϵ is the relative abundance by number of each species, and μ is its molecular weight. A partial atlas of the spectrum showing the best-fit model and marking the positions of all lines with equivalent widths in the model greater than 5 m\AA is shown in Figs. A.1 – A.3.

3.1 Previous work

The above measurements of T_{eff} and g are sufficiently discrepant from those by Vennes et al. (2011) and Németh et al. (2012) to require comment. Although the

LTE to be small except for very strong lines; the same is expected to be true here, and is evident in the final best-fit model.

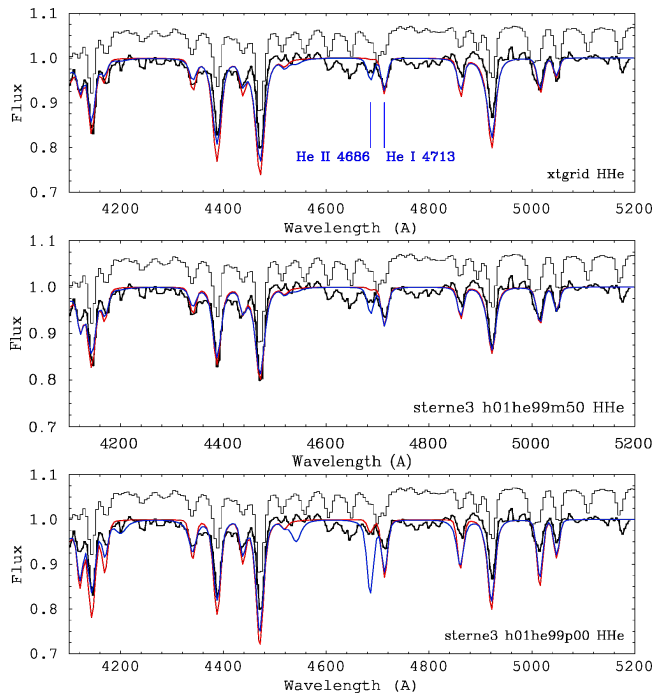


Figure 2. Part of the EFOSC/NTT spectrum of J1845–4138 (bold black), normalised and compared with different model atmosphere predictions. In all three panels, the model spectra are for $(T_{\text{eff}}/\text{kK}, \log g/\text{cm s}^{-2}, n_{\text{He}}/n_{\text{H}}) = (26.0, 5.0, 100)$ (red) and $(36.0, 5.5, 100)$ (blue). The top panel shows model spectra from a grid of non-LTE H+He models (Nemeth et al. 2014). The middle panel uses models computed using STERNE3 with abundances of all elements other than H and He set to 0. The bottom panel uses models computed using STERNE3 with abundances of all elements other than H and He set to solar values; the emergent spectrum includes H+He lines only. The SALT-HRS spectrum is also shown, degraded to resolution 13\AA and offset vertically (light black).

EFOSC/NTT spectra is of very low resolution, it is sufficient to resolve the adjacent He I 4713 Å and He II 4686 Å lines, which provide a critical temperature diagnostic at these temperatures. The online plot⁴ of the Németh et al. (2012) fit to J1845–4138 shows both lines; although the fit is not perfect, the line ratio implies that the model at $T_{\text{eff}} = 36\text{ kK}$ is consistent with the observation. The shape of the flux distribution is only a weak constraint since, for hot stars in the optical and near-ultraviolet, it is degenerate with the shape of interstellar extinction.

The key to the discrepancy lies in a large systematic difference between the degree of metal-line blanketing in the model atmospheres. Vennes et al. (2011) used non-LTE model atmospheres consisting of hydrogen and helium only. Németh et al. (2012) included carbon, nitrogen and oxygen, and obtained a very similar T_{eff} . The omission of opacity from other ions, especially iron-group elements, has a major impact on the temperature structure of the model photosphere. This impact is further enhanced in hydrogen-deficient atmospheres owing to the absence of the normally dominant hydrogen photoionisation and the halving of the

electron-scattering opacity (recall that $\kappa_{\text{es}} = \kappa_{\text{es},0}/\mu_e = 0.20(1 + X)$, where μ_e is the number of nucleons per free electron and X is the hydrogen mass fraction). The STERNE3 models are fully line blanketed and include opacity contributions from all major ions through to the iron-group and beyond (Behara & Jeffery 2006).

The consequence is illustrated in Fig. 2, where three model classes including (1) non-LTE H+He only, (2) LTE H+He only, and (3) LTE H+He+solar metals are compared. Two models are compared in each class, having $T_{\text{eff}} = 26$ and 36 kK . The helium to hydrogen ratio is close to 100 in each case. The non-LTE models were taken from the grid of (Nemeth et al. 2014)⁵. The LTE models were computed with STERNE3 (Behara & Jeffery 2006). To enable a proper comparison, the emergent spectra include H and He lines only. It is instructive to find (at this resolution) only minor differences between the non-LTE and LTE spectra where no metals are included in the model atmosphere calculation. A very substantial shift in the He I/He II ionization balance occurs when metals are included. This is due to the backwarming effect of metal-line opacity which heats the lower layers of the atmosphere and increases the degree of ionization in the line forming region at a given T_{eff} . Hence He II 4686 Å appears at much lower T_{eff} in fully-blanketed H-deficient models than it does in models which either have more hydrogen or lower metallicity. As demonstrated emphatically by Anderson & Grigsby (1991) when discussing diagnostics for the atmospheres of normal B stars, it is essential to include all opacity sources before considering departures from LTE except, possibly, at the very lowest surface gravities.

4 DISCUSSION

With $V = 14.6$, J1845–4138 is 4 magnitudes fainter than V652 Her. Its measured T_{eff} and g imply L/M approximately 3 times smaller. It is dangerous to infer a mass from putative evolutionary tracks for such stars. Jeffery (1988) discussed core-mass shell-luminosity relations for helium-shell stars, but even assuming a simple relation of the form $L \propto M^\delta$ is problematic since δ varies strongly with mass. Assuming $M \approx 0.5 M_\odot$, then $L \approx 350 L_\odot$ (with large errors). Also assuming extinction of 0.23 mag. for this position (Schlafly & Finkbeiner 2011)⁶ and a bolometric correction -2.50 mag. , appropriate for early B stars, yields a distance $d \approx 4.4\text{ kpc}$. With galactic coordinates $l^{ii} = 354.1900$, $b^{ii} = -16.6900$, this gives a location half way toward the Galactic bulge, with height $z \approx 1.4\text{ kpc}$ below the plane.

The spectroscopic similarities with V652 Her argue for a similar evolutionary status; in that case the model most consistent with observations (including pulsations) is that of a post double helium white dwarf merger (Saio & Jeffery 2000; Zhang & Jeffery 2012). Tracks for models of such stars are shown in Fig. 3. If the same is true here, J1845–4138 will evolve to become a helium and nitrogen-rich hot subdwarf within 10^5 y or so. The enrichment of nitrogen and depletion of carbon point to a highly CNO-processed helium surface; some hydrogen from surface layers of the progenitor

⁴ <http://stelweb.asu.cas.cz/~nemeth/work/galex/catalog/>

⁵ http://www.ster.kuleuven.be/~petern/work/sd_grid/

⁶ <http://irsa.ipac.caltech.edu/applications/DUST/>

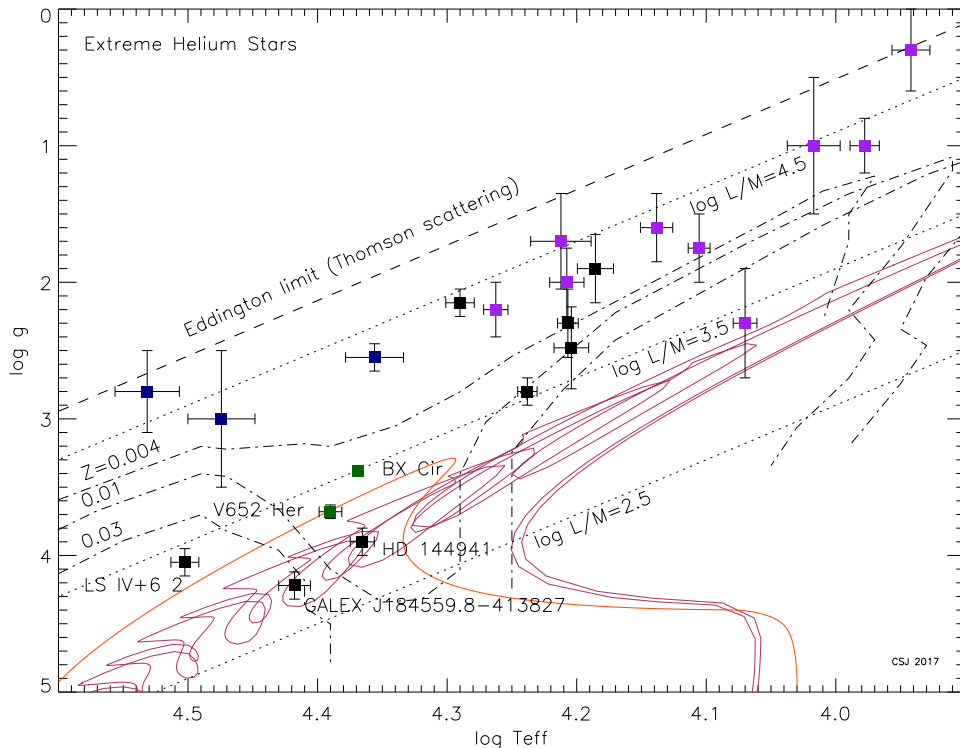


Figure 3. The $g - T_{\text{eff}}$ diagram for all known extreme helium stars, including J1845–4138. The positions of the Eddington limit (Thomson scattering; dashed), luminosity-to-mass contours (solar units: dotted) and lower boundaries for pulsation instability (metallicities $Z = 0.004, 0.01, 0.03$: dot-dashed) (Jeffery et al. 1999) are also shown. In the online version, variable EHe’s are shown in purple (cool), blue (hot), green (V652 Her like variables). Non-variables are black. Data for T_{eff}, g are as in Jeffery (2008), except for BD+10°2179 (Kupfer et al. 2017). Post-merger evolution tracks for models of He+He white dwarf mergers (Zhang & Jeffery 2012, 0.30+0.25 and 0.30+0.30 M_{\odot}) are shown in maroon. Part of the post-flash track of a 0.46921 M_{\odot} ‘late hot flasher’ (metallicity $Z = 0.01$) is shown in orange (Miller Bertolami et al. 2008).

white dwarfs has survived (Hall & Jeffery 2016). The photospheric iron abundance is subsolar (≈ 0.4 dex), but not low enough to be considered ‘metal-poor’. The merger of a CO white dwarf and a helium white dwarf is predicted to produce a carbon-rich surface, having negligible hydrogen (typically $< 0.01\%$ by number), and a much higher L/M ratio than observed in the current case (Saio & Jeffery 2002).

A second class of model which might apply to such stars includes the ‘late hot flasher’ models wherein helium-core ignition occurs some time after a star leaves the red giant branch (Brown et al. 2001; Miller Bertolami et al. 2008); if the remaining hydrogen envelope is sufficiently thin, flash-driven convection can enrich the surface with CNO-processed helium as well as carbon. The evolution track for a $Z = 0.01, 0.46921 M_{\odot}$ model is shown in Fig. 3. Neither model satisfactorily accounts for the mass loss required for the star to leave the giant branch before helium ignition, unless assisted by a binary or planetary companion. Brown et al. (2001) predicted high carbon abundances. Miller Bertolami et al. (2008) found a range of surface mixtures from (for example) high carbon (4% by mass, initial metallicity $Z = 0.01$), negligible nitrogen at high mass (0.47725 M_{\odot}), to moderate carbon (1.2%) and nitrogen (2.1%) at lower mass (0.46644 M_{\odot}), for models with deep mixing, of which the 0.47725 M_{\odot} model passes closest

to the position of J1845–4138. There is no evidence that this class of models can produce pre-subdwarfs with CNO-cycled helium surfaces and without carbon enrichment.

There is a clear distinction between the nitrogen-rich, carbon-poor surface of J1845–4138 and the carbon-rich surfaces of all EHe’s other than V652 Her (Jeffery et al. 2011, Table 1), where the mean carbon abundance is ≈ 2.5 dex higher than in J1845–4138. The same is true of all RCrB stars, to which high luminosity EHe’s are thought to be related, though the difference here is ≈ 2 dex (ibid.). Three other relatively hot ‘high-gravity’ helium stars are shown in Fig. 3 and Table 1. LS IV+6°2 and BX Cir are both carbon-rich and hydrogen-poor relative to V652 Her and J1845–4138. HD144941 is more hydrogen-rich and extremely metal poor. It is not clear how or whether these stars are related to one another. Amongst helium-rich hot subdwarfs, there exists a range of carbon abundance from $\log \epsilon_{\text{C}} = 6.73 \pm 0.18$ (SB 21) to 8.94 (BPS CS 29496–0010), whilst the nitrogen abundances are clustered around $\log \epsilon_{\text{N}} \approx 8.4$ (Hirsch & Heber 2009; Naslim et al. 2010).

The question of whether J1845–4138 also pulsates has yet to be determined; J1845–4138 lies outside the region where radial pulsations driven by the Z-bump opacity mechanism are predicted (Jeffery & Saio 1999). Due to its smaller radius, any radial or p-mode pulsation period

must be shorter than that of V652 Her (0.108 d). There is no evidence of any periodic variability in the All Sky Automated Survey (ASAS) catalogue entry for this object (Pojmanski & Maciejewski 2005). Since the ASAS cadence is $< 1\text{d}^{-1}$, this is not a strong non-detection.

A remarkable property of J1845–4138 is the sharpness of its absorption lines. This places strong constraints on both the rotation velocity and the microturbulent velocity in the photosphere. One question posed by the hypothesis for its origin in a white dwarf merger origin is how J1845–4138 could have lost so much angular momentum during the immediate post-merger evolution. On the other hand, a significant number of helium-enriched subdwarf B stars are being identified with very low rotation velocities (Naslim et al. 2011, 2013; Jeffery et al. 2017).

5 CONCLUSION

SALT HRS observations of a faint-blue star previously classified He-sdB (Vennes et al. 2011) demonstrate it to be a nitrogen-rich EHe star similar to the pulsating EHe star V652 Her. J1845–4138 becomes the first EHe star to be discovered for nearly 40 years, indicative of the extreme rarity of these stars. Its surface is predominantly that of CNO-processed helium with some hydrogen contamination, pointing to a possible origin in a double helium white dwarf merger. The Galactic position and metallicity of J1845–4138 are compatible with membership of the bulge population. This discovery suggests that there are more EHe stars waiting to be found, at least with relatively low luminosities. A higher signal-to-noise spectrum will allow abundances and other parameters to be refined further.

ACKNOWLEDGMENTS

The observation reported in this paper was obtained with the Southern African Large Telescope (SALT) under program 2016-2-SCI-008 (PI: Jeffery). The author is indebted to the hard work of the entire SALT team. He thanks Peter Németh for a copy of the reduced EFOSC/NTT spectrum of J1845–4138.

The Armagh Observatory is funded by direct grant from the Northern Ireland Dept of Communities. CSJ acknowledges support from the UK Science and Technology Facilities Council (STFC) Grant No. ST/M000834/1.

This research has made use of the SIMBAD database, operated at CDS, Strasbourg, France.

REFERENCES

- Ahmad A., Jeffery C. S., Fullerton A. W., 2004, *A&A*, 418, 275
- Anderson L., Grigsby J. A., 1991, in Crivellari L., Hubeny I., Hummer D. G., eds, *NATO Advanced Science Institutes (ASI) Series C Vol. 341 of NATO Advanced Science Institutes (ASI) Series C, Line Blanketing Without LTE - the Effect on Diagnostics for B-Type Stars*. p. 365
- Asplund M., Grevesse N., Sauval A. J., Scott P., 2009, *ARA&A*, 47, 481
- Beers T. C., Doinidis S. P., Griffin K. E., Preston G. W., Shectman S. A., 1992, *AJ*, 103, 267
- Behara N. T., Jeffery C. S., 2006, *A&A*, 451, 643
- Bianchi L., Conti A., Shiao B., 2014, *Advances in Space Research*, 53, 900
- Bramall D. G., Sharples R., Tyas L., et al. 2010, in *Ground-based and Airborne Instrumentation for Astronomy III Vol. 7735 of Proc. SPIE, The SALT HRS spectrograph: final design, instrument capabilities, and operational modes*. p. 77354F
- Brown T. M., Sweigart A. V., Lanz T., Landsman W. B., Hubeny I., 2001, *ApJ*, 562, 368
- Buckley D. A. H., Swart G. P., Meiring J. G., 2006, in *Society of Photo-Optical Instrumentation Engineers (SPIE) Conference Series Vol. 6267 of Proc. SPIE, Completion and commissioning of the Southern African Large Telescope*. p. 62670Z
- Şener H. T., Jeffery C. S., 2014, *MNRAS*, 440, 2676
- Crause L. A., Sharples R. M., Bramall D. G., et al. 2014, in *Ground-based and Airborne Instrumentation for Astronomy V Vol. 9147 of Proc. SPIE, Performance of the Southern African Large Telescope (SALT) High Resolution Spectrograph (HRS)*. p. 91476T
- Crawford S. M., Crause L., Depagne É., et al. 2016, in *Ground-based and Airborne Instrumentation for Astronomy VI Vol. 9908 of Proc. SPIE, Data reductions and data quality for the high resolution spectrograph on the Southern African Large Telescope*. p. 99082L
- Dreizler S., Heber U., Werner K., Moehler S., de Boer K. S., 1990, *A&A*, 235, 234
- Drilling J. S., 1996, in Jeffery C. S., Heber U., eds, *Hydrogen Deficient Stars Vol. 96 of Astronomical Society of the Pacific Conference Series, Basic data on hydrogen-deficient stars*. p. 461
- Drilling J. S., Bergeron L. E., 1995, *PASP*, 107, 846
- Drilling J. S., Hill P. W., 1986, in Hunger K., Schönberner D., Kameswara Rao N., eds, *Hydrogen Deficient Stars and Related Objects, Proceedings of IAU Colloq. 87 Vol. 128 of Astrophysics and Space Science Library, Appendix a : a Catalogue of Hydrogen Deficient Stars*. D. Reidel Publishing Co, Dordrecht, p. 499
- Drilling J. S., Jeffery C. S., Heber U., 1998, *A&A*, 329, 1019
- Drilling J. S., Jeffery C. S., Heber U., Moehler S., Napitowitzki R., 2013, *A&A*, 551, A31
- Green R. F., Schmidt M., Liebert J., 1986, *ApJS*, 61, 305
- Greenstein J. L., Sargent A. I., 1974, *ApJS*, 28, 157
- Hagen H.-J., Groote D., Engels D., Reimers D., 1995, *A&AS*, 111, 195
- Hall P. D., Jeffery C. S., 2016, *MNRAS*, 463, 2756
- Harrison P. M., Jeffery C. S., 1997, *A&A*, 323, 177
- Hirsch H., Heber U., 2009, *Journal of Physics Conference Series*, 172, 012015
- Husfeld D., Butler K., Heber U., Drilling J. S., 1989, *A&A*, 222, 150
- Jeffery C. S., 1988, *MNRAS*, 235, 1287
- Jeffery C. S., 1998, *MNRAS*, 294, 391
- Jeffery C. S., 2008, *Information Bulletin on Variable Stars*, 5817, 1
- Jeffery C. S., Baran A. S., Behara N. T., et al. 2017, *MNRAS*, 465, 3101
- Jeffery C. S., Harrison P. M., 1997, *A&A*, 323, 393

- Jeffery C. S., Hill P. W., Heber U., 1999, *A&A*, 346, 491
- Jeffery C. S., Karakas A. I., Saio H., 2011, *MNRAS*, 414, 3599
- Jeffery C. S., Kurtz D., Shibahashi H., Starling R. L. C., Elkin V., Montañés-Rodríguez P., McCormac J., 2015, *MNRAS*, 447, 2836
- Jeffery C. S., Saio H., 1999, *MNRAS*, 308, 221
- Jeffery C. S., Woolf V. M., Pollacco D. L., 2001, *A&A*, 376, 497
- Justham S., Podsiadlowski P., Han Z., 2011, *MNRAS*, 410, 984
- Kawka A., Vennes S., O’Toole S., Németh P., Burton D., Kotze E., Buckley D. A. H., 2015, *MNRAS*, 450, 3514
- Kupfer T., Przybilla N., Heber U., Jeffery C. S., Behara N. T., Butler K., 2017, *MNRAS*, submitted
- Miller Bertolami M. M., Althaus L. G., Unglaub K., Weiss A., 2008, *A&A*, 491, 253
- Moehler S., de Boer K. S., Heber U., 1990, *A&A*, 239, 265
- Naslim N., Geier S., Jeffery C. S., Behara N. T., Woolf V. M., Classen L., 2012, *MNRAS*, 423, 3031
- Naslim N., Jeffery C. S., Ahmad A., Behara N. T., Şahin T., 2010, *MNRAS*, 409, 582
- Naslim N., Jeffery C. S., Behara N. T., Hibbert A., 2011, *MNRAS*, 412, 363
- Naslim N., Jeffery C. S., Hibbert A., Behara N. T., 2013, *MNRAS*, 434, 1920
- Németh P., Kawka A., Vennes S., 2012, *MNRAS*, 427, 2180
- Nemeth P., Östensen R., Tremblay P., Hubeny I., 2014, in van Grootel V., Green E., Fontaine G., Charpinet S., eds, 6th Meeting on Hot Subdwarf Stars and Related Objects Vol. 481 of Astronomical Society of the Pacific Conference Series, Synthetic Spectra for O and B Type Subdwarf Stars. p. 95
- Pandey G., Lambert D. L., 2011, *ApJ*, 727, 122
- Pérez-Fernández E., Ulla A., Solano E., Oreiro R., Rodrigo C., 2016, *MNRAS*, 457, 3396
- Pojmanski G., Maciejewski G., 2005, *Acta Astron.*, 55, 97
- Popper D. M., 1942, *PASP*, 54, 160
- Przybilla N., Butler K., Heber U., Jeffery C. S., 2005, *A&A*, 443, L25
- Reindl N., Rauch T., Werner K., Kruk J. W., Todt H., 2014, *A&A*, 566, A116
- Saio H., Jeffery C. S., 2000, *MNRAS*, 313, 671
- Saio H., Jeffery C. S., 2002, *MNRAS*, 333, 121
- Schlafly E. F., Finkbeiner D. P., 2011, *ApJ*, 737, 103
- Schulz H., Wegner G., Heber U., 1991, *PASP*, 103, 435
- Stobie R. S., Kilkenny D., O’Donoghue D., et al. 1997, *MNRAS*, 287, 848
- Ströer A., Heber U., Lisker T., Napiwotzki R., Dreizler S., Christlieb N., Reimers D., 2007, *A&A*, 462, 269
- Vennes S., Kawka A., Németh P., 2011, *MNRAS*, 410, 2095
- Wisotzki L., Koehler T., Groote D., Reimers D., 1996, *A&AS*, 115, 227
- York D. G., Adelman J., Anderson Jr. J. E., et al. 2000, *AJ*, 120, 1579
- Zhang X., Jeffery C. S., 2012, *MNRAS*, 419, 452

APPENDIX A: SPECTRAL ATLAS FOR J1845–4138

Figures A.1 to A.3 contain a partial atlas of the *SALT HRS* spectrum of J1845–4138 with the best model fit and identifications of absorption lines.

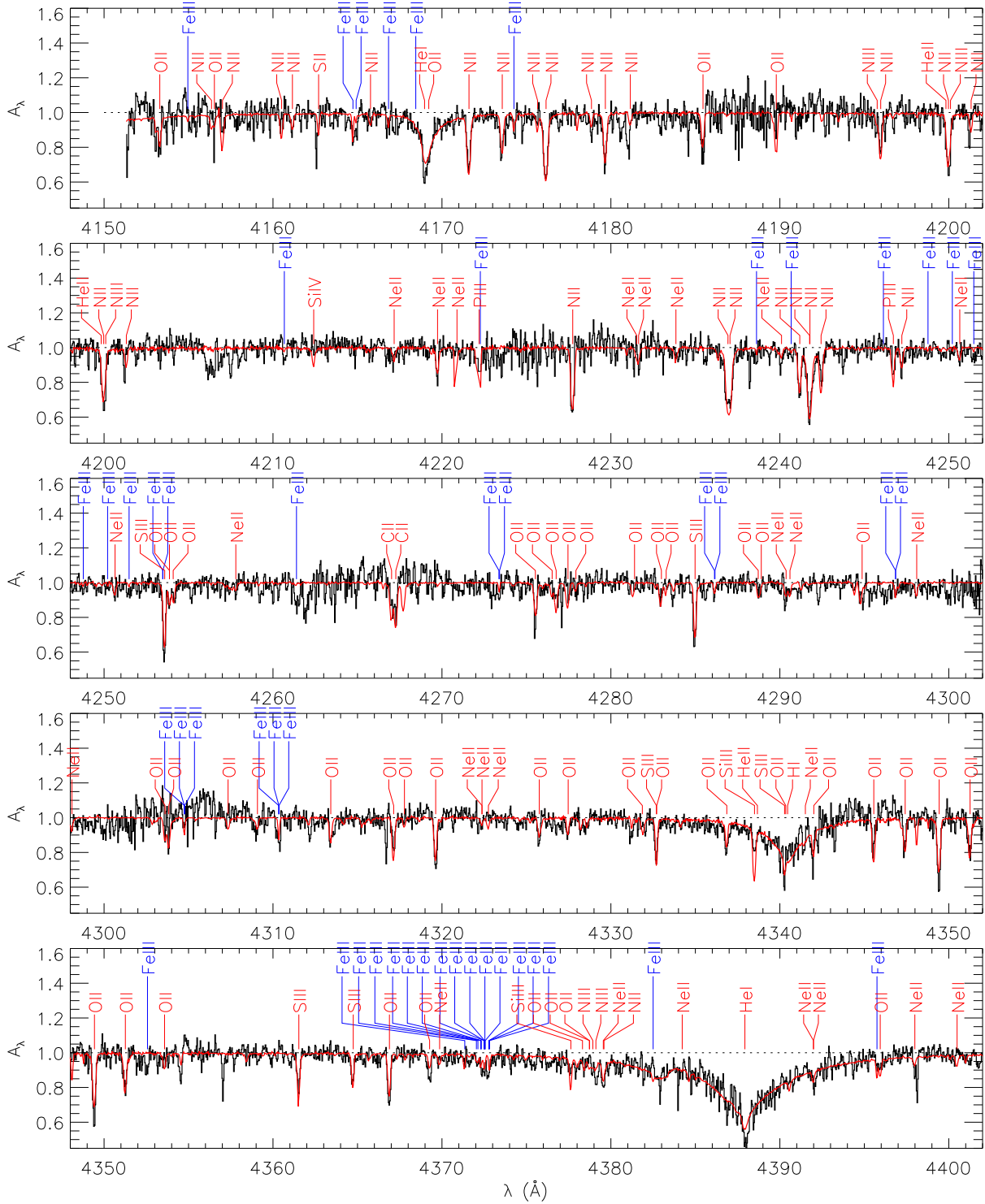


Figure A.1. Parts of the observed SALT HRS spectrum of J1845–4138 (black histogram), and the best-fit model having $T_{\text{eff}} = 26\,000\text{ K}$, $\log g/\text{cm s}^{-2} = 4.2$, $n_{\text{H}}/n_{\text{He}} = 0.01$ and abundances shown in Table 1 (red polyline). Lines with theoretical equivalent widths greater than 5 mÅ are identified wherever possible. Apparently large bins in the observed spectrum correspond to major instrumental artefacts; other artefacts appear as very sharp regularly-spaced lines.

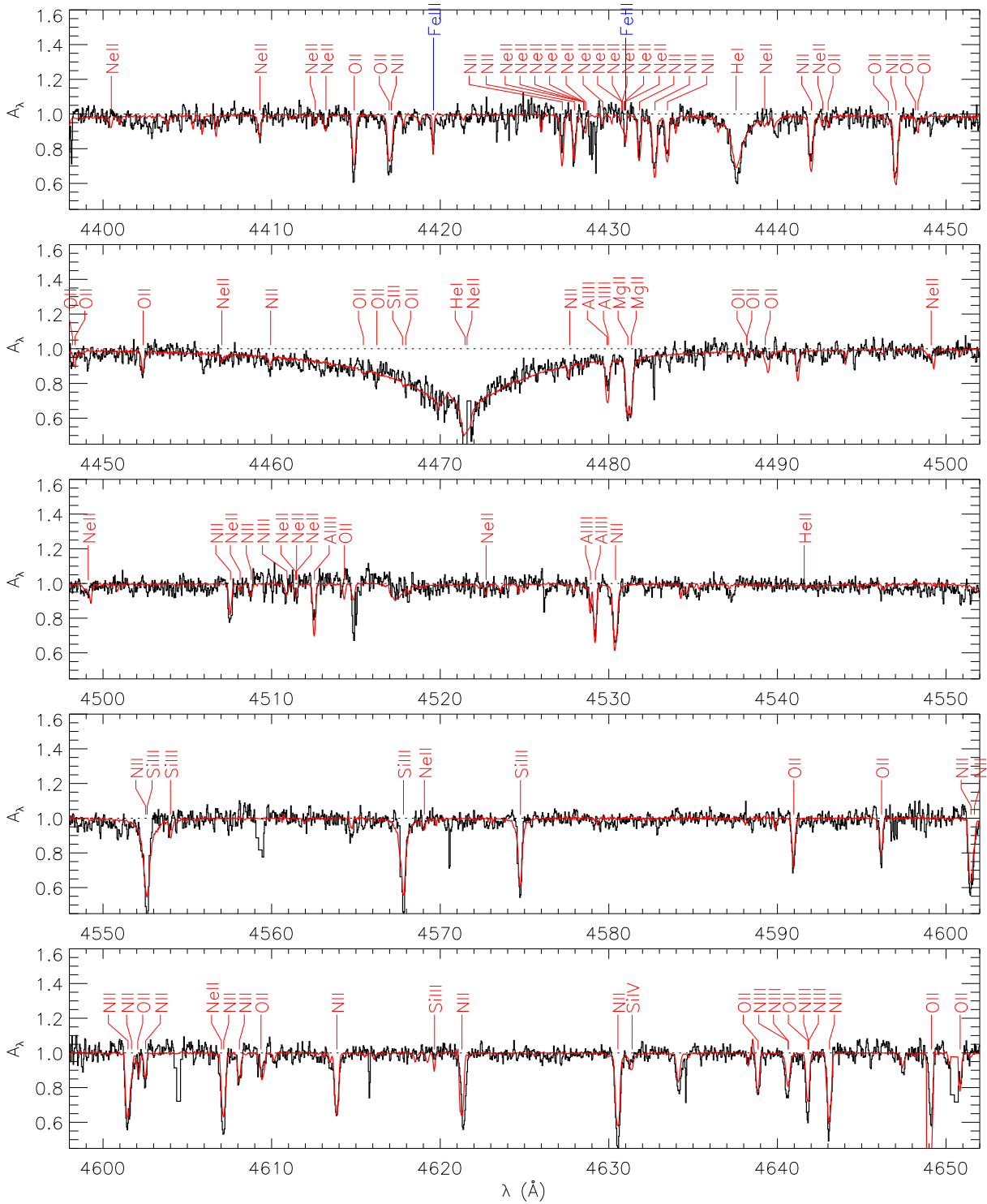


Figure A.2. As Fig. A.1 (contd.)

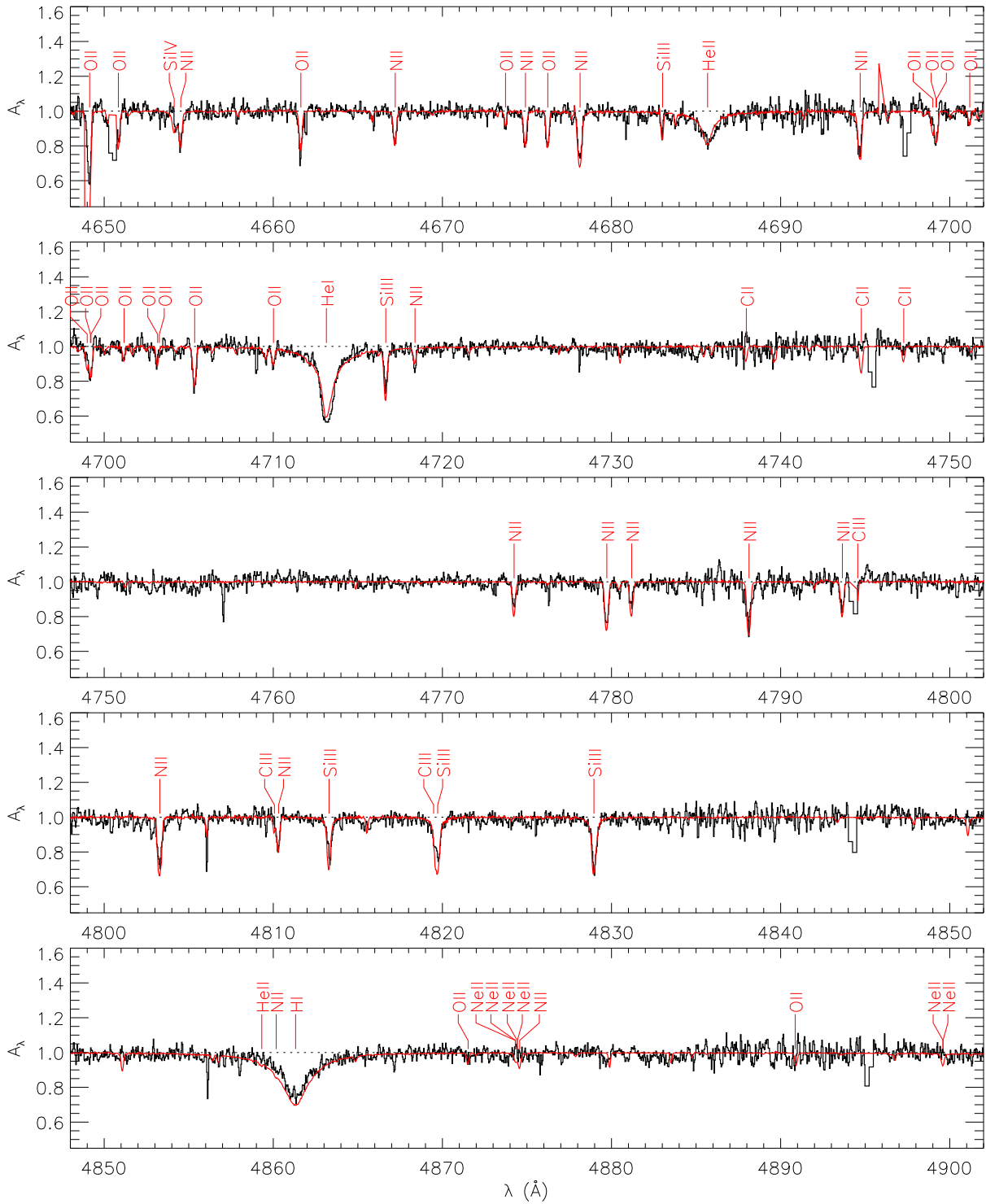


Figure A.3. As Fig. A.1 (contd.)